Micromechanical Analysis of Cement Paste with Carbon Nanotubes

Vít Šmilauer, Petr Hlaváček, Pavel Padevět

Czech Technical University in Prague, Faculty of Civil Engineering, Department of Mechanics, Thákurova 7, 166 29 Prague 6, Czech Republic

Corresponding author: vit.smilauer@fsv.cvut.cz

Abstract

Carbon nanotubes (CNT) are an attractive reinforcement material for several composites, due to their inherently high strength and high modulus of elasticity. There are controversial results for cement paste with admixed CNT up to 500 µm in length. Some results show an increase in flexural or compressive strength, while others showing a decrease in the values. Our experiments produced results that showed a small increase in fracture energy and tensile strength. Micromechanical simulations on a CNT-reinforced cement paste 50×50 µm proved that CNT clustering is the crucial factor for an increase in fracture energy and for an improvement in tensile strength.

Keywords: carbon nanotubes, cement hybrid material, micromechanics, fracture energy.

1 Introduction

Worldwide production of cement has increased significantly in recent years, due to the growing demand for concrete. In 2010, $3.3 \cdot 10^9$ tons of cement were produced, which is three times the quantity of $1.1 \cdot 10^9$ tons produced in 1990. For reasons of sustainability and profitability, secondary cementitious materials have been introduced into the binder, reducing the amount of Portland clinker in the cement. A further reduction can be made if the strength of the hydrated cement increases.

Carbon nanofibers (CNF) and carbon nanotubes (CNT) are a feasible approach to the production of a high strength binder, as has been demonstrated for composites [3, 19] and specifically for cement pastes [2, 4, 5, 9, 12]. Theoretical and experimental studies have indicated that CNT exhibit Young modulus from 180 to 588 GPa and tensile strength in the range between 2000 and 6140 MPa [10]. Both CNT and CNF as admixtures are very difficult to distribute uniformly, even within a small volume of cement paste. Flocculation make it impossible to obtain improved properties of composite materials, unless a special treatment is applied.

It is a challenging task to achieve good dispersion of CNT/CNF in a cement matrix. A simple powder mixing procedure leads to poor dispersal of the carbon nanomaterials in a cement paste. For this reason, Sanchez and Ince proposed adding silica fume to cement to increase the dispersiveness of CNF [15]. Dispersion of CNT/CNF in water using surfactants is another method, and is a widely-used way to introduce carbon nanomaterials into polymers [2]. However, most surfactants and additives interfere with the hydration reaction of cement, and usually prolong the cement setting and hardening times.

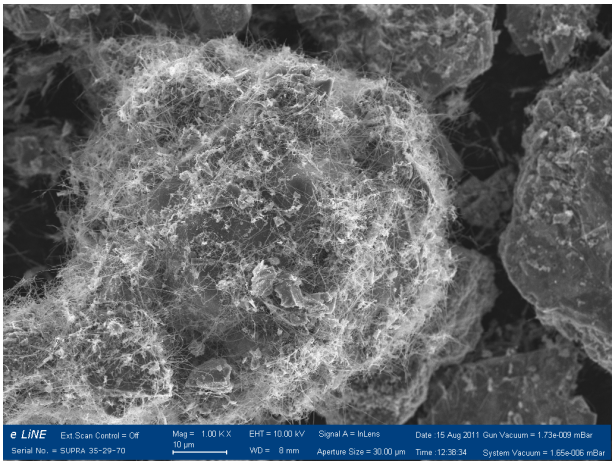

Figure 1: CNT synthesized on the surface of a cement grain. The image is 115 µm in width. Image by K. Hruška, Institute of Physics ASCR, Prague.

Another way to enhance the dispersiveness of CNT/CNF is by functionalizing them. The carboxyl or hydroxyl groups attached to the surface of carbon that form during oxidation treatment can create bonds between the matrix and carbon nanomaterials. Functionalized CNT have already been proven to influence the mechanical properties of hydrated cement paste [2, 5].

Another method uses CNT directly synthesized on the surface of cement grains [12], see Figure 1. Cement hybrid material (CHM) of this type can easily be blended with conventional cement. This procedure guarantees dispersion of CNT in the cement matrix. It has been reported that even a small mass fraction of CNT/cement = 0.005 helped to increase flexural strength by 22 % [5].

CNT length (μm)	w/c	Compressive s. (MPa) Plain	CNT	Flexural s. (MPa) Plain	CNT	Ref.
< 10	P 0.30	38.3 ± 8.2	61.8 ± 0.8	2.3 ± 0.4	2.3 ± 0.2	[2]
< 30	P 0.30	—	—	9.2	12.6	[4]
$< \sim 10$	M 0.40	28.9	54.3	6.0	8.23	[8]
< 500	P 0.45	52.3 ± 0.7	62.1 ± 1.4	6.7 ± 0.1	8.4 ± 0.2	[5]
< 100	P 0.50	—	—	5.5	7.2	[9]
$< \sim 5$	P —	49	56	16	8	[12]

Table 1: Summary of published data on strength gain when CNT is added to cement. P-paste, M-mortar.

Reports on improvement of compressive and flexural strength when un/functionalized CNT is added to a cement paste are inconsistent across the literature. For example, a decrease of more than 30 % in compressive strength has been reported [2]. Table 1 shows the most optimistic claimed improvements which were achieved by adding certain amounts of CNT/CNF to cement paste or mortar, measured after 28 days of hardening.

In addition, data from Table 1 demonstrates that even CNT shorter than 10 μm can be effective in providing added strength. This raises the question of the reinforcing mechanism. To shed the light on the mechanical effect of CNT, a series of experimental data was measured and micromechanical simulations were executed. The results are presented below.

2 Experiments

2.1 Materials

Ordinary Portland cement CEM I 42.5 R from Mokrá, Czech Republic, was used as the source material for all specimens. The specific Blaine surface was 306 m^2/kg, the chemical composition of the relevant elements was CaO 65.6 %, SiO_2 19.0 %, Fe_2O_3 3.5 %, MgO 1.1 % by mass.

Cement hybrid material (CHM) with grown CNT on the surface was synthesized by a group from Aalto University, Finland, under the leadership of L. Nasibulina by the chemical vapor deposition method [13]. CNT growth occurred at about 600°C in a fluidized bed reactor, where acetylene served as the main carbon source due to its low decomposition temperature and its affordable price. The CNT grown on the cement particles are approximately 30 nm in diameter and up to 3 μm in length [11], and the specific surface area of CNT is about 10–20 m^2/g.

CHM has density 2.59 kg/m^3 and contains 30 % of carbon by mass, which occupies 43 % of the volume.

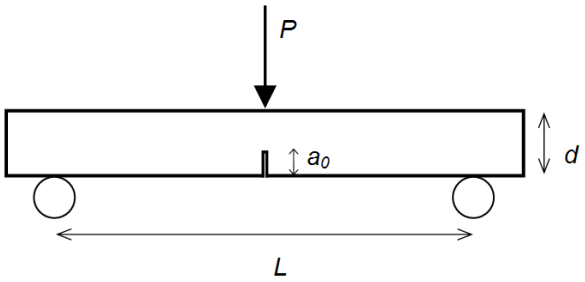

Figure 2: Layout of the three-point bending test used for fracture energy determination.

Table 2 summarizes the compositions of five experimental batches with the same water/binder ratio of 0.35. The batches cover feasible mixes potentially usable in concrete engineering. 0.2 % Glenium ACE 40 superplasticizer was added to the binder mass. The superplasticizer contains 65 % of water by mass, which was deducted from the total amount of water.

2.2 Casting and curing of the specimens

Hand stirring of each batch took three minutes, and consecutive vibration and form filling took an additional period of four minutes. Specimens $40 \times 40 \times 80$ mm in size were covered, and after 24 hours they were cured in a water bath at ambient temperature. At 30 days of hardening, the specimens were cut with a diamond saw into nine parts with approximate dimensions $13 \times 13 \times 80$ mm.

The production of such small-size specimens by cutting from larger bodies is more efficient than direct casting into small molds. The casting and vibration of a small amount of material was found to be ineffective, and the quality of the specimens (including surface defects or material inhomogeneity) is significantly worse than the quality attained by hand-cutting from larger bodies.

Designation (mass %)	CEM I (g)	CHM (g)	Water (g)	Carbon/paste (vol %)
CEM 100 % + CHM 0 %	234.0	0	81.9	0
CEM 96.5 % + CHM 3.5%	225.81	8.19	81.9	0.88
CEM 93 % + CHM 7 %	217.62	16.38	81.9	1.75
CEM 86 % + CHM 14 %	201.24	32.76	81.9	3.47
CEM 70 % + CHM 30 %	163.8	70.2	81.9	7.31

Table 2: Five batches of cement pastes with different amounts of CHM.

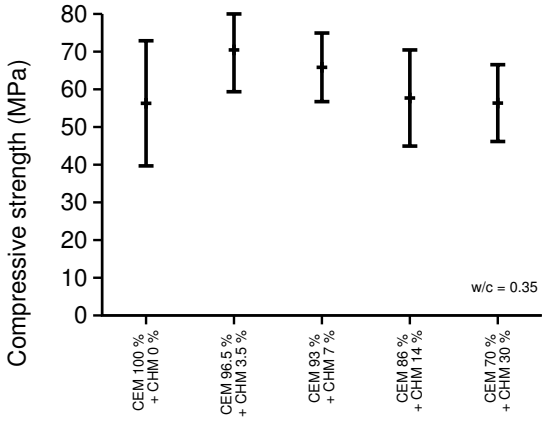

Figure 3: Compressive strength of a plain paste and pastes with admixed CHM.

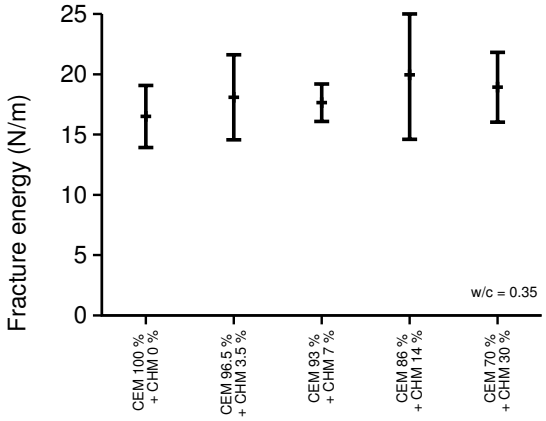

Figure 4: Fracture energy of a plain paste and pastes with admixed CHM.

In accordance with RILEM standards for mechanical testing [17], notches were cut in the middle of the beams to 45 % of the depth for subsequent fracture energy determination.

2.3 Determining the mechanical properties

The fracture energy, G_f, was determined according to the RILEM standard [17], see Figure 2 for the experimental scheme. At least five notched beams from one batch were used to obtain the statistical results.

The three-point bending test under a displacement-controlled regime gave access for the full load displacement curve on an MTS Aliance RT 30 electromechanical machine. The work of external force P is calculated as

$$W_f = \int_0^{u_f} P \, \mathrm{d}u \tag{1}$$

where u is the load-point displacement and u_f represents the final displacement at which the load is equal to zero. The average (effective) fracture energy in the ligament, according to the RILEM standard, is defined as

$$G_f = \frac{W_f}{b(d - a_0)} \tag{2}$$

where b is the thickness of the beam, d is the beam depth, and a_0 is the depth of the notch. The support span L was set to 50 mm.

The compressive strength was determined from two broken pieces of each beam. Thick metal pads 13×13 mm were put on the top and bottom surfaces, and the peak force was recalculated to the compressive strength.

2.4 Experimental results

Figure 3 shows the compressive strength of the hardened pastes at 30 days after the casting. Replacing 3.5 % cement with CHM leads to a 25 % increase in compressive strength, in our case from an average value of 56 MPa to an average of 70 MPa. This paste contains only 0.88 % of CNT by volume. Increased CHM dosage leads to a slight decrease in compressive strength.

Figure 4 depicts the evolution of fracture energy. The CHM samples exhibit an increase in fracture

Component	E (GPa)	ν	f_t (MPa)	G_f (N/m)
Porosity	0.2	0.02	—	—
Clinker	135	0.3	1800	118.5
Products	21.7	0.24	5.58	11.5
CNT	231	0.14	3000	200

Table 3: Elastic and fracture properties of the components.

energy even in a small amount of replacement. Replacing 3.5 % of the cement by CHM causes a 14 % increase in the fracture energy.

It should be added that a variation in CHM content has consequences for workability, paste density and porosity. The results indicate that the classical CNT pull-out or crack bridging mechanism does not occur. Microcrack shielding seems to be the most relevant mechanism operating in hardened cement paste reinforced by short CNT, giving only a slight increase in the fracture energy [7]. In contrast, PVA-reinforced cement-based composites with fibers several millimeters in length yield fracture energy that is higher by orders of magnitude [6]. This experimental finding is further supported by micromechanical simulations that show a certain increase in the upper-bound fracture energy.

3 Micromechanical simulations

2D micromechanical simulations aimed to reproduce the fracture energy from CNT-free and CNT-reinforced cement pastes and, in addition, to explore the role of clustering and CNT length. The CEMHYD3D cement hydration model generated the 3D microstructure of hydrated cement paste, from which a 2D slice 50×50 µm was taken. Various chemical phases were reduced to three components; capillary porosity, clinker minerals and hydration products, which correspond mainly to C-S-H. For 30 days of hydration, the volume fractions yield to 14.2 %, 11.6 % and 74.2 % respectively. The CNT volume fraction was considered as 3.47 %, which corresponds to a composition of CEM 86 % + CHM 14 %.

CNT fibers were introduced as 1D truss elements, connecting particular nodes of 2D quadrilateral elements. Each fiber is represented by one finite element without intermediate hanging nodes, in order to simplify the model.

An isotropic damage material model is assigned to all four components. A simple cohesive crack model with linear strain softening and Mazars' measure of strain is used:

$$\sigma = (1-\omega)E\varepsilon = f_t\left(1 - \frac{h\omega\varepsilon f_t}{2G_f}\right), \tag{3}$$

$$\tilde{\varepsilon} = \sqrt{\sum_{I=1}^{3}\langle\varepsilon_I\rangle^2}, \tag{4}$$

where σ is the normal stress transferred across a cohesive crack, f_t is the uniaxial tensile strength, h is the effective width of a finite element, ε is the normal strain to a crack, G_f is the mode-I fracture energy, and ω is the damage parameter. $\langle\varepsilon_I\rangle$ are positive parts of the principal values of the strain tensor ε. Equation (3) leads to an explicit evaluation of damage parameter ω.

Table 3 summarizes the elastic and fracture properties of the four components. The elastic modulus of porosity was assigned a finite value, since this speeds up convergence. It was checked that a further reduction of the modulus leads to negligible changes in results. Clinker minerals are crystalline phases with high tensile strength and normally suffer no damage during loading. Their fracture energy is recalculated from scratch-test results [18].

The properties of CNT are estimated on the basis of recent results [16]. Hydration products, mainly C-S-H, are taken as the low-density type of C-S-H [1]. The C-S-H tensile strength and the C-S-H fracture energy were deduced from experimental data and a 2D simulation of plain paste. These two parameters were identified by means of an inverse-problem, taking the most reasonable case of the two weakly dependent parameters; flexural strength assuming 5.8 MPa, similar to [5, 8], and for fracture energy assuming 16.5 N/m as determined from our lab tests, see Figure 4.

Figure 5 depicts microstructure images for micromechanical simulations. As mentioned above, a composition of CEM 86 % + CHM 14 % was considered for all cases, with the exception of plain paste. The cross-section of one CNT truss element was 50 nm times 1 µm, which in fact represents a bundle of CNT, not a single nanotube. The CNT length was randomized according to uniform distribution and length limit. The orientation of the CNT fibers is also random. Gaussian distribution of CNT fibers in a cluster was

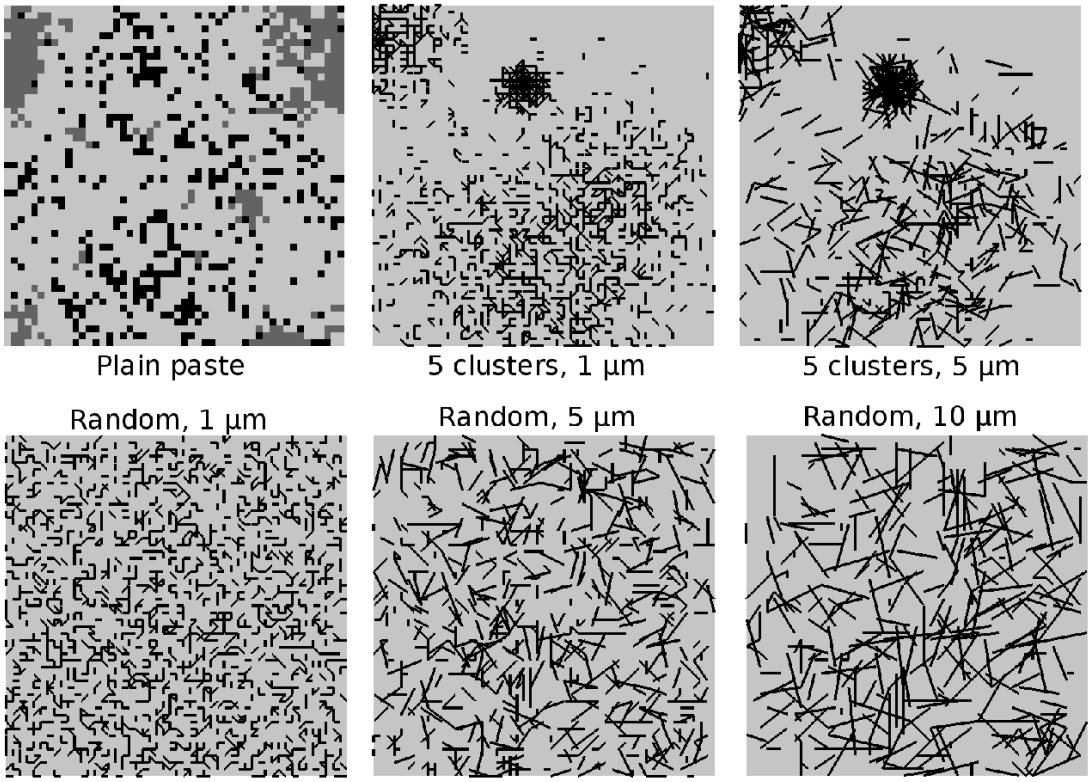

Figure 5: 2D microstructures used in the simulations. The plain paste contains three phases (black — porosity, dark gray — clinker minerals, light gray — hydration products). Other subfigures show CNT fibers distributed within plain paste, either in clusters or randomly.

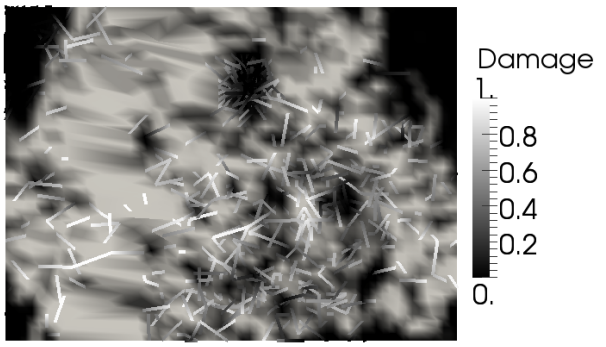

Figure 6: Deformed microstructure with 5 clusters and CNT length up to 5 µm before the peak load.

used, and the cluster radius is uniformly distributed up to 10 µm.

The subfigures in Figure 5 show CNT fibers distributed in the paste. Each pixel was assigned to a quadrilateral element with four nodes, so the mesh is uniform and easily generated. Each simulation leads to 4900 unknown displacements, contains 150 displacement increments, uses the modified Newton-Raphson solver, and runs for approximately 5 minutes in the OOFEM package [14].

Figure 6 elucidates the damage distribution in the microstructure of 5 clusters with CNT length up to 5 µm before the peak load. Note that there is no paste damage inside the heavily CNT-reinforced zones.

CNT clusters	CNT length	f_t (MPa)	G_f (N/m)
Plain paste	Plain paste	5.8	16.5
5	≤ 1 µm	5.9	15.5
5	≤ 5 µm	6.3	25.9
0 (no clusters)	≤ 1 µm	6.3	27.7
0 (no clusters)	≤ 5 µm	7.1	43.8
0 (no clusters)	≤ 10 µm	7.3	55.8

Table 4: Elastic and fracture properties of CNT-reinforced paste.

Table 4 summarizes the results from micromechanical simulations. It is evident that clustering of CNT is the most critical factor. Clustering leads to crack formation around strongly-reinforced zones, which renders the CNT reinforcement ineffective. The simulations show that the uniform distribution of 1 µm CNT increases G_f from 16.5 to 27.7 N/m. Clustering leads to a smaller increase, even with CNT 5 µm in length.

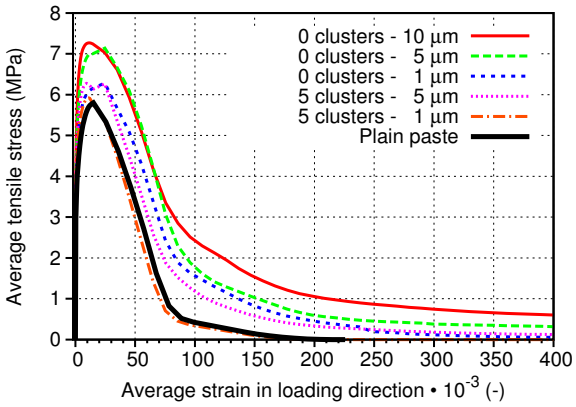

Figure 7: A stress-strain diagram for loaded microstructures.

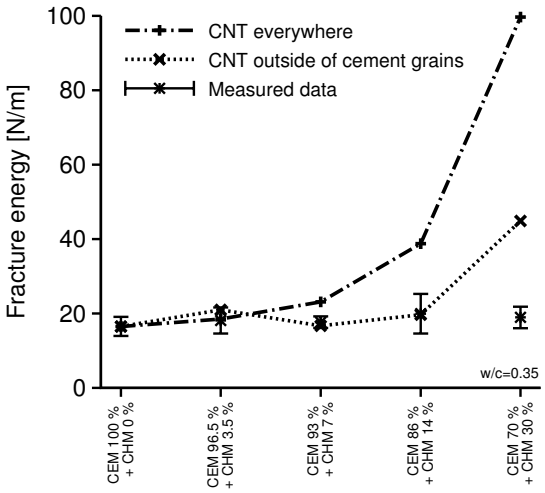

Figure 8: Fracture energy of pastes with variable CHM content (CNT length up to 3 µm). Micromechanical simulations with average CNT length up to 2.5 µm consider CNT placement everywhere or only in areas outside of originally unhydrated cement grains.

Figure 7 plots the stress-strain diagram for plain and CNT-reinforced pastes. Note that there is not much increase in flexural strength but there is a significant improvement in ductility, which is reflected as an increase in fracture energy.

Addition of CNT to cement paste, in any form, leads necessarily to clustering. According to the Powers model of cement hydration, the CNT-unreinforced volume corresponds to the initial volume of unhydrated cement grains, where CNT cannot enter during initial mixing. The initial volume fraction of the clinker corresponds to

$$f_{\text{clinker}} = \frac{0.32}{w/c + 0.32}, \tag{5}$$

which for $w/c = 0.35$ yields 48 %. This large volume remains unreinforced and prevents uniform distribution of CNT fibers. This explains why our experimental fracture energy is always lower than when micromechanical predictions with a uniform CNT distribution are used.

Further simulations with variable CHM content support the hypothesis that CNT clustering lowers the amount of fracture energy. Figure 8 shows that placing CNT only outside of originally unhydrated cement grains corresponds well with the experimental results. Cement paste with 30 % CHM shows discrepancy with micromechanical simulation, the reason lies probably in lower workability and extensive CNT separation during mixing.

4 Conclusions

The role of CNT reinforcement in cement paste provides another option for improving the quasi-brittle behavior of cementitious materials. Experimental evidence shows a marginal improvement in compressive strength and fracture energy. As has been proven by numerical simulations, the clustering of CNT in the paste microstructure is the crucial factor, due to the presence of unreacted cement grains in the initial mixture and the intermixing of CHM with ordinary cement. However, micromechanical simulations show that a uniform distribution CNT fibers only 1 µm in length may increase the fracture energy from 16.5 to 27.7 N/m, and the flexural strength up to 10 %.

Direct synthesis of CNT on the surface of cement particles solved the problem with flocculation of CNT separately added to the cement paste, but the problem of initially unhydrated grains remained. The claimed twofold increase in the compressive strength of cement paste with added CNT was not proven by our experiments [8]. Preliminary micromechanical simulations indicate that a real CNT reinforcement is ineffective when the tubes are shorter than an average cement grain. Hence, an effective CNT reinforcement needs to be at least approximately 15 µm CNT in length. The appropriate length of CNT reinforcement will be a topic for further research.

Acknowledgements

We gratefully acknowledge financial support from the Ministry of Education and Youth of the Czech Republic under CEZ MSM 6840770003, and from the Czech Science Foundation GAČR under projects P104/12/0102 and 103/09/H078.

References

[1] G. Constantinides, F.-J. Ulm. The effect of two types of C-S-H on the elasticity of cement-based materials: Results from nanoindentation

and micromechanical modeling. *Cem Concr Res* **34**(1):67–80, 2004.

[2] A. Cwirzen, K. Habermehl-Cwirzen, V. Penttala. Surface decoration of carbon nanotubes and mechanical properties of cement/carbon nanotube composites. *Advances in cement research* **20**(2):65–74, 2008.

[3] E. Hammel, X. Tang, M. Trampert, et al. Carbon nanofibers for composite applications. *Carbon* **42**(5-6):1153–1158, 2004.

[4] Maria S. Konsta-Gdoutos, Zoi S. Metaxa, Surendra P. Shah. Multi-scale mechanical and fracture characteristics and early-age strain capacity of high performance carbon nanotube/cement nanocomposites. *Cement and Concrete Composites* **32**(2):110–115, 2010.

[5] Geng Ying Li, Pei Ming Wang, Xiaohua Zhao. Mechanical behavior and microstructure of cement composites incorporating surface-treated multi-walled carbon nanotubes. *Carbon* **43**(6):1239–1245, 2005.

[6] Victor C. Li, H. Horii, P. Kabele, et al. Repair and retrofit with engineered cementitious composites. *Engineering Fracture Mechanics* **65**(2–3):317–334, 2000.

[7] Victor C. Li, Mohamed Maalej. Toughening in Cement Based Composites. Part I: Cement, Mortar, Concrete. *Cement and Concrete Composites* **18**(4):223–237, 1996.

[8] Péter Ludvig, José M. Calixto, Luiz O. Ladeira, Ivan C. P. Gaspar. Using converter dust to produce low cost cementitious composites by in situ carbon nanotube and nanofiber synthesis. *Materials* **4**(3):575–584, 2011.

[9] Z. S. Metaxa, M. S. Konsta-Gdoutos, S. P. Shah. Mechanical Properties and Nanostructure of Cement Based Materials Reinforced with Carbon Nanofibers and PVA Microfibers. *ACI Special Publication 270: Advances in the Material Science of Concrete SP-270-10* **270**:115–124, 2010.

[10] P. Morgan. *Carbon fibers and their properties*. CRC Press, 2005. 794-796.

[11] Prasantha R. Mudimela, Larisa I. Nasibulina, Albert G. Nasibulin, et al. Synthesis of carbon nanotubes and nanofibers on silica and cement matrix materials. *Journal of Nanomaterials*, 2009.

[12] Albert G Nasibulin, Sergey D Shandakov, Larisa I Nasibulina, et al. A novel cement-based hybrid material. *New Journal of Physics* **11**(2):023013, 2009.

[13] Larisa I. Nasibulina, Ilya V. Anoshkin, Sergey D. Shandakov, et al. Direct synthesis of carbon nanofibers on cement particles. *Transportation Research Record: Journal of the Transportation Research Board* **2**(2142):96–101, 2010.

[14] B. Patzák, Z. Bittnar. Design of Object Oriented Finite Element Code. *Advances in Engineering Software* **32**(10–11):759–767, 2001.

[15] Florence Sanchez, Chantal Ince. Microstructure and macroscopic properties of hybrid carbon nanofiber/silica fume cement composites. *Composites Science and Technology* **69**(7–8):1310–1318, 2009.

[16] V Šmilauer, C. G. Hoover, Z. P. Bažant, et al. Multiscale Simulation of Fracture of Braided Composites via Repetitive Unit Cells. *Engineering Fracture Mechanics* **78**(6):901–918, 2011.

[17] RILEM TC50-FMC. Determination of the fracture energy of mortar and concrete by means of three-pointbend tests on notched beams. *Materials and Structures* **18**(4):285–290, 1985.

[18] F.-J. Ulm, R. Pellenqs. Bottom–up materials science. In *MIT-France Energy Forum*. 2011.

[19] B. I. Yakobson, C. J. Brabec, J. Bernholc. Nanomechanics of carbon tubes: Instabilities beyond linear response. *J Phys Rev Lett* **76**(14):2511–2515, 1996.